OPERATING RANGES OF METEOROLOGICAL WIND TUNNELS FOR THE SIMULATION OF CONVECTIVE BOUNDARY LAYER PHENOMENA

by

Robert N. Meroney, Professor
Civil Engineering Department
Colorado State University
Fort Collins, Colorado 80523, USA

and

William H. Melbourne, Professor
Mechanical Engineering Department
Monash University
Clayton, Victoria 3168, Australia

submitted to

Journal of Boundary-Layer Meteorology

December 10, 1991

CEP90-91-RNM-WNM-11

Table of Contents

List of Symbols

A_J, A_T, A_i	Emperical coefficients for dynamic sublayer characteristics
B_J, B_T, B_i	Emperical coefficients for dynamic-convective sublayer characteristics
C	Concentration
C_J, C_T, C_i	Emperical coefficients for free convection sublayer characteristics
D_s	Stack diameter
F, G	Dimensionless integrals from augmented velocity and temperature profile expresssions
F_s	Stack plume buoyancy flux
F_*	Stack buoyancy parameter for CBL situations
Fr_m	Modified Froude Number
g	Gravitational constant
h_s	Stack height
L	Stratification length scale
L_{mo}	Monin-Obukhov length scale
L_*	Dynamic sublayer characteristic depth scale
L_{**}	Dynamic-convective sublayer characteristic depth scale
L_{ASL}	Atmospheric surface layer characteristic depth scale
LSR	Prototype to model length scale ratio
MR	Stack exhaust momentum ratio
Q	Surface heat flux
Q_s	Stack exhaust flow rate
Re	Reynolds number
Ri_B	Bulk Richardson number
Ri_*	Surface heat flux Richardson number

Ri_s	Surface mass flux Richardson number
$(Ri_*)_{eff}$	Effective Richardson number
T	Temperature
T^*	Dimensionless temperature
T_*	Characteristic mixing layer temperature
u_*	Friction velocity
u_{**}	Dynamic-convective velocity scale
U	Mean longitudinal velocity
U_m	Mean mixed layer velocity
U^*	Dimensionless velocity
w_*	Convection velocity
W	Mean vertical velocity
W_s	Stack exhaust velocity
W^*	Dimensionless vertical velocity
x, y, z	Coordinates
z_i	Inversion height
δz_i	Interfacial entrainment layer depth
z_u, z_T	Surface roughness lengths for velocity and temperature profiles, respectively
β	Buoyancy parameter, $g\gamma$
γ	Coefficient of thermal expansion, $1/T_o$
Γ	Temperature gradient above inversion
κ	Von Karman constant
ϕ_u, ϕ_T	Dimensionless velocity and shear, respectively
ζ	Dimensionless vertical height, z/L
θ	Potential temperature
θ_*	Surface layer temperature scale

σ_u, σ_v, σ_w, σ_t Turbulence variances of velocity and temperature

Subscripts

m	model
p	prototype
s	stack
w	wall

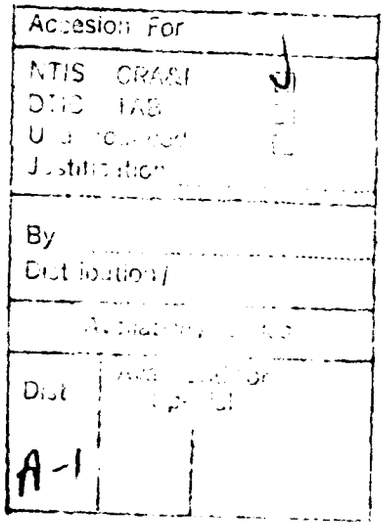

OPERATING RANGES OF METEOROLOGICAL WIND TUNNELS FOR THE SIMULATION OF CONVECTIVE BOUNDARY LAYER PHENOMENA

R.N. Meroney[1] and W.H. Melbourne[2]

[1]Department of Civil Engineering, Colorado State University
Fort Collins, Colorado, 80523, U.S.A.

[2]Department of Mechanical Engineering, Monash University
Clayton, Victoria, 3168, Australia

Abstract: The operating ranges of meteorological wind tunnels for convective boundary layer (CBL) simulation are defined in this paper based on a review of the theoretical and practical limitations of the flow phenomena and the facilities available. Wind-tunnel operating ranges are limited by the dimensions of the simulated circulations and of the tunnel itself, the tunnel flow speed and turbulence processes, and the characteristics of the measurement instrumentation. When it is desired to simulate both the convective boundary layer and the behavior of other flows imbedded within the boundary layer, such as power-plant plume rise and dispersion, then additional constraints exist on the fluid modeling process. The capabilities of meteorological wind tunnels can also be extended through the judicious use of boundary and side wall flow controls.

1. Introduction

Convective boundary layer (CBL) circulations are surface temperature-forced atmospheric circulations observed almost daily over most of the earth's surface. An understanding of the convective boundary layer (CBL) has only begun to emerge from laboratory, field and numerical research in the last twenty years. Recent studies have focused on the characteristics of the large and central mixed layer, but still unresolved are the details of how the various CBL sublayers are linked together. Much of the remaining difficulties relate to the fact that definitive measurements in regions above the meteorological tower heights but below the mixed layer and above the mixed layer within the capping entrainment layer are difficult to acquire.

Much of today's understanding of the CBL has come from convection tank and laboratory studies. Conventional type and size water tank and wind tunnel facilities provided data which were used to interpret the mixed-layer atmospheric physics and to validate analytic and numerical models for plume behavior. Routine engineering investigations of CBL impact on power-plant plumes or other activities of man will be constrained by the inherent limitations of the size and type of simulations used. This paper examines some of the limitations of fluid modeling and critiques the potential for boundary-layer control methods to extend the capabilities of existing meteorological wind tunnels.

a. Global Characteristics of the CBL

Predictions of many features of neutral and stable atmospheric boundary layers were made possible through Lagrangian similarity assumptions (Monin and Obukhov, 1954), K-modeling and mixing length numerical approaches, and even laboratory simulation in air and water facilities (Arya and Plate, 1969). Initially it was hoped that the Monin-Obukhov similarity approach would also explain the vagaries of the unstable boundary layer, but, as height increased above ground level, data departed significantly from predictions. Then Willis and Deardorff (1974) performed a series of experiments on the behavior of stably stratified water layers heated from below in a water tank, and they found that the characteristic

length, velocity and temperature scales were the mixing layer depth, z_i, the convective velocity, w_*, and the convective temperature, θ_*, respectively; where

$$w_* = \left[\frac{gQz_i}{\rho C_p T_a}\right]^{1/3} \quad \text{and} \quad \theta_* = \qquad .$$

Earlier, based on sub-grid scale modeling of unstable channel flow, Deardorff (1970, 1972) had suggested this possibility existed for situations where $-z_i/L_{mo} > 10$.

Caughey (1984) and Kader and Yaglom (1990) suggest that the convective boundary layer may be idealized as a multilayer structure. Proceeding upwards from the surface one can identify 1) the dynamic sublayer in which shear plays a dominant role such that all velocities and lengths scale with friction velocity, u_*, and position, z. This layer persists as long as the production of shear produced vertical fluctuation energy is less than buoyant production of such motions [$z < L_* = (\kappa u_*)^3/(Q\beta)$]. Next 2) the dynamic-convective sublayer denotes a region where horizontal velocities are scaled by the characteristic shear velocity, u_* but vertical motions scale by the convective velocity, w_*. The upper edge of the dynamic-convective sublayer is at a height z of the order $L = \kappa L_{mo}$. When $z > L_{**} = (\kappa_1 u_*)^3/(Q\beta)$ then shear stress, τ_o, is no longer important but height continues to be the significant length scale. In this 3) free convection sublayer the characteristic velocity for all directions becomes the convective velocity, w_*. Somewhere around $z = 0.1z_i$ the free convection sublayer blends into the 4) mixed layer for which the relevant length, velocity, and temperature scales are now mixed layer depth, z_i, convective velocity, w_*, and convective temperature, θ_*. Finally between $0.8z_i$ and $1.2z_i$ exists the 5) entrainment interfacial layer which depends upon the convective velocity, w_*, the depth of the capping inversion, and the strength of the stable flow aloft.

b. The Mixed Layer

Deardorff and Willis (1975) predicted diffusion phenomena in convective boundary layers based on laboratory experiments and sub-grid scale modeling calculations. They found that plume behavior was completely unlike Gaussian dispersion models. Subsequent modeling approaches for dispersion in the mixed layer are reviewed by Lamb in Nieustadt and van Dop (1984). The most successful models have adopted a Lagrangian viewpoint and use sub-grid scale modeling. Some investigators argue that popular approaches of Reynolds stress closure do not work well, because such models fail to take into account the three-dimensional effects of general subsidence which accompanies the rise of thermals from the ground.

As stated by Lamb (1984) "*the long life times of updrafts and downdrafts make it very frequently possible for diffusing particles to traverse the entire depth of the mixed layer in one steady motion. This is incompatible with the tenets of Eulerian K-theory, in which turbulent diffusion is envisaged as a brownian motion or random walk type process in which particles can traverse large distances after suffering many upward and downward displacements...for this reason, dispersion parameters derived for convective conditions from K-theory principles are unreliable...Even second order closure models are likely to yield erroneous predictions of concentration in the mixed layer.*" Nonetheless, Rodi (1986) has

recently argued kinetic-energy-closure models can still "effectively" reproduce temperature distribution and mixing-layer depth variations with time. These features, however, will not be sensitive to the affect of subsidence and updrafts on isolated polluted plumes.

c. The Near-wall Sublayers

The earliest results concerning the turbulence structure of the regions beneath the "mixed layer" are due to Prandtl (1932). Later other researchers such as Obukhov (1946, 1960), Monin & Obukhov (1954) and Priestly (1954, 1960) developed his ideas further and made them more precise. The arguments used to describe the near-ground flow were based on similarity and conventional dimensional arguments. They suggested that shear, temperature and turbulence characteristics could be described in certain layers by various power-law expressions made up of scaling variables and z within the limits of unidentified universal constants. Two layers were identified--a near wall region where fluid properties were expected to vary as $\zeta = z/L$ when $(0 < \zeta < 1)$:

$$dU/dz = u_*/(\kappa z)\ \phi_U(\zeta), \quad dT/dz = -T_*/z\ \phi_T(\zeta),$$

$$\sigma_u = u_*\phi_1(\zeta), \ \sigma_v = u_*\phi_2(\zeta), \ \sigma_w = u_*\phi_3(\zeta),$$

$$\sigma_t = T_*\ \phi_4(\zeta), \text{ etc.}$$

and a free convection region where thermal gradients and moments were expected to be independent of u_* when $\zeta >> 1$:

$$dU/dz = B_U u_*^2 (Q\beta)^{-1/3} z^{-4/3} \quad \text{or} \quad \phi_U = B_U \zeta^{-1/3},$$

$$dT/dz = -B_T Q^{2/3} \beta^{-1/3} z^{-4/3} \quad \text{or} \quad \phi_T = -B_T \zeta^{-1/3},$$

$$\sigma_u = C_1 (Q\beta z)^{1/3}, \ \sigma_t = C_4 Q^{2/3} (\beta z)^{-1/3}, \text{ etc.}$$

Initially, it appeared that such expressions when combined with mixed-layer scaling described the unstably stratified environment quite well, but then several inconsistencies became apparent:

1. The free-convection expressions appeared to correlate data at unexpectedly small values of ζ down to 0.1,

2. Agreement of shear and temperature gradients with the derived expressions were rather poor as ζ got larger than 2 or 3,

3. It was not clear why the expression for dU/dz in the free-convection layer should contain u_*, while the other expressions were independent of this variable, and, finally,

4. Measurements for <ut> and <uwt> did not agree with the proposed expressions at all!

Based on the concepts of "directional" or "vector" or "anisotropic" dimensional analysis Betchov and Yaglom (1971) proposed a three-layer model for the

atmospheric surface layer which lies beneath the mixed layer. This less conventional analysis technique proposes that horizontal and vertical scales of motion and velocity should be scaled by separate variables. Therefore it permits one to obtain sharper results than those implied by conventional dimensional analysis. In some cases it requires an increase in the list of parameters of a problem (the additional parameter is not necessary if horizontal and vertical motions are energetically uncoupled.)

The three sublayers and their limits were described above. Dimensional arguments show that each layer requires its own unique shear, temperature and turbulence parameterization and correlations. In the dynamic sublayer where buoyancy effects can be neglected the well-known logarithmic formulae for U and $\bar{T}$ are valid:

$$U(z) = u_*/\kappa \ln(z/z_U), \quad T(z) = T_*/\kappa \ln(z/z_T),$$

$$\sigma_u = A_1 u_*, \quad \sigma_v = A_2 u_*, \quad \sigma_w = A_3 u_*,$$

$$\sigma_t = A_4 T_*, \text{ etc.}$$

where T_* is the wall temperature and z_U and z_T are surface roughness coefficients.

But in the dynamic-convective sublayer the velocity scales are described by a vertical scale $w_* = (Q\beta z)^{1/3}$ and a horizontal scale $u_{**} = u_*^2/w_*$, and a temperature scale $\theta_* = Q/w_*$, which result in expressions:

$$dU/dz = B_U u_{**}/z = B_U u_*^2 (Q\beta)^{-1/3} z^{-4/3} \text{ or } \phi_U = B_U \zeta^{-1/3},$$

$$dT/dz = -B_T \theta_*/z = -B_T Q^{2/3} \beta^{-1/3} z^{-4/3} \text{ or } \phi_T = -B_T \zeta^{-1/3},$$

$$\sigma_u = B_1 u_*^2 (Q\beta z)^{-1/3}, \quad \sigma_v = B_2 u_*^2 (Q\beta z)^{-1/3}, \quad \sigma_w = B_3 (Q\beta z)^{1/3},$$

$$\sigma_t = B_4 \theta_* = B_4 Q^{2/3} (\beta z)^{-1/3}, \text{ etc.}$$

Then in the free-convection sublayer only w_* and θ_* are required such that:

$$dU/dz = C_U w_*/z = C_U (Q\beta)^{1/3} z^{-2/3} \text{ or } \phi_U = C_U \zeta^{1/3},$$

$$dT/dz = -C_T \theta_*/z = -C_T Q^{2/3} \beta^{-1/3} z^{-4/3} \text{ or } \phi_T = C_T \zeta^{-1/3},$$

$$\sigma_u = C_1 (Q\beta z)^{1/3}, \quad \sigma_v = C_2 (Q\beta z)^{1/3}, \quad \sigma_w = C_3 (Q\beta z)^{1/3},$$

$$\sigma_t = C_4 Q^{2/3} (\beta z)^{-1/3}, \text{ etc.}$$

Unfortunately, the data available in 1971 was insufficient in scope or quality to confirm these expressions. As a result the concepts lay dormant until 1990 when Kader and Yaglom reported the results from new atmospheric measurements made in Russia during the mid-1980s. As noted in Figure 1 derived from their paper the new data confirmed the non-monotonicity of the function ϕ_U, which had never been noticed before. They uncovered strong evidence for the existence of all

three sublayers and even proposed values for many of the universal constants:

$$A_U \approx 2.5\ ,\ A_T \approx 2.4,\ B_U \approx 1.7\ ,\ B_T \approx 1.1,$$

$$C_U \approx 0.7\ ,\ C_T \approx 0.9,$$

$$A_1 \approx 2.7\ ,\ A_2 \approx 2.5,\ A_3 \approx 1.25,\ A_4 \approx 2.9,$$

$$B_3 \approx 1.65,\ B_4 \approx 1.4$$

$$C_3 \approx 1.3\ ,\ C_4 \approx 1.5.$$

Indeed Kader and Yaglom were even able to suggest coefficient values for some of the higher third-order moments like $\langle w^2 t \rangle$, $\langle uw^2 \rangle$, $\langle uwt \rangle$, etc. and the dissipation rate, ϵ.

The behavior of the functions in the transition regions between the various sublayers can not be found from dimensional reasoning, but empirical formulae can be fitted to the data, for example:

$$\phi_U(\zeta) = 2.5\left[\frac{1 + 0.1\zeta^2}{1 + 3\,\zeta}\right],\quad \phi_T(\zeta) = 1.6\left[\frac{3 + \zeta}{1 + 4\zeta + 8\zeta^2}\right].$$

Such expressions can be integrated over a range of ζ values to produce predictive expressions for the velocity and temperature profiles as noted in Figures 2 and 3.

d. Entrainment Interfacial Layer

The rate of propagation of the mixed layer into the stably stratified layer above is perhaps the least well understood of the mixing phenomena which occur in the CBL. Since the process takes place in a relatively thin layer involving the penetration, propagation, breaking and dissipation of internal waves it has been singularly unavailable to accurate measurement. Nonetheless, many analytic and numerical models have been proposed based on simplistic laboratory measurements to explain the phenomena. Since the time scales of this process are rather long compared to those of the layers below, it is often possible to study the two regions separately. Meteorologists, oceanographers, limnologists and solar pond engineers have all focused on interfacial layer behavior through such simulations (Wyngaard, 1988; Atkinson and Harleman, 1983; Iwasa et al., 1988).

Nonetheless, such assumptions are by no means always permitted. Entrainment-induced turbulence can extend down through the mixed layer to the surface, particularly in the case of humidity (Wyngaard, 1988). The entrainment flux at the CBL top can exceed that at the surface. Thus one must be careful when inferring fluxes of momentum or heat from measurements of other variables, especially in the surface layers.

Most laboratory experiments to date have been performed in small apparatus sized from centimeters to a meter in depth. These experiments have contributed a great deal, but they leave unresolved questions about Reynolds number similarity

constraints and the details of mixing processes too small to resolve at such scales.

2. Laboratory Simulation of the CBL

Much of the understanding of the CBL has come from convection tank and large eddy simulation (LES) studies. The original work by Willis and Deardorff (1974) is now complimented by wind-tunnel measurements taken at Colorado State University (Arya and Plate, 1969; Poreh and Cermak, 1984), and the soon to be published work by Sawford and Hibbard of the Atmospheric Research Division, CSIRO Aspendale, Australia. Sawford and Hibbard are using a salt-water analogue to the thermal CBL process to simulate mixing layer phenomena.
Thermally stratified wind tunnels currently exist at Colorado State University, USA (2 m x 2 m cross-section, 30 m long) and at the National Institute for Environmental Studies, Japan (2 m x 3 m cross-section, 24 m long). New wind-tunnel facilities specifically designed to study the CBL are under construction or evaluation at the Central Electricity Generating Facility, Leatherhead, UK (1.5 x 3.5 m cross-section, 20 m long), the Ecole Centrale de Lyon, France (2 x 3.7 m cross-section, 15 m long), Karlsruhe University, BRD (0.5 x 1 m cross-section, 4 m long), and the very ambitious facility at Monash University, Australia (5 m x 10 m cross-section, 40 m long). At this time no results have been published based on experiments performed in these new facilities.

a. Water-Tank Experiments

Laboratory experiments in water tanks have contributed substantially to a better understanding of convectively mixed layers. Experiments with such facilities continue to contribute important information about the mixed layer and its rates of growth. Visualization experiments performed with laser sheets and chemically fluorescing plumes yields detailed information about the mixing characteristics of buoyant plumes in the CBL. These studies clearly demonstrate that the process is non-Gaussian.

Small size limits the spatial resolution characteristics of most water tank simulation of the CBL. Typical mixed layer depths examined are from 0.1 to 0.5 m deep; hence, the equivalent atmospheric surface layer regions are below 1 cm, and the stability length, L, may be at most of the order of millimeters. It is unlikely then that CBL water tank measurements will contribute substantially to a better understanding of the atmospheric surface layer (ASL) where the three-sublayers reside.

Deeper entrainment layers may be produced in larger water tank facilities. For example the Stratified Mixing Facility at Colorado State University consists of a 2 m deep, 10 m long tank provided with thick side wall insulation, floor heating, recirculation pumps, a salt water filling system, visualization windows, and temperature and concentration measurement instrumentation.

b. Wind-Tunnel Experiments

Deardorff (1972) showed for the CBL that when $-z_i/L_{mo} > 10$ (Note: Arya (1982) suggests > 5), then turbulence scales with the mixing layer depth, z_i, and the convective velocity, w_*. Characteristic distributions of temperature, T, velocity, U, and heat flux, <wt>, are sketched in Figure 4. Time is expected to scale as tw_*/z_i, vertical distance should scale as z/z_i, horizontal distance as $xw_*/(z_i U_m)$, and concentration as $Cz_i^2 U_m/Q_s$ or $C_r z_i U_m/Q_s$. Assuming undistorted vertical and horizontal scales, this means one must maintain model and prototype w_*/U_m equivalent.

Once the mixing layer depth and convective velocity scales are stipulated for the laboratory experiment, it is also necessary that the rate of mixing layer growth $(dz_i/dt)/w_*$ be similar. Unfortunately, for convenient model velocities, eg., $U_m \approx 1$ to 2 m/s, very large surface heat fluxes may be required, eg., 200 to 15,000 watts/m^2, and intense stable temperature gradients at the top of the mixing layer, eg. $dT/dz \approx 50$ to 2000 °C/m. An alternative approach to the creation of an elevated inversion which might be adequate is to use the upper wind-tunnel roof as the effective inversion height, z_i. The validity of this approach must be examined carefully, however, since a downward flux of heat due to interfacial entrainment plays an important role in many mixed layer characteristics.

3. Laboratory Simulation of Atmospheric Transport in the CBL

Simulation of the behavior of industrial plumes released into the CBL require the additional equality of plume exit momentum ratio,

$$MR = \rho_s W_s^2 D_s^2/(\rho U^2 z_i^2),$$

and the ratio of plume exit buoyancy to free-stream momentum,

$$Fr_m = g\Delta\rho D_s W_s/(\rho U^3),$$

sometimes called the modified Froude number. The joint stipulation that the velocity ratio, w_*/U, length ratio, D_s/z_i, and modified Froude number, Fr_m, are similar is equivalent to equality of the buoyancy parameter, F_*, defined as the ratio of plume exit buoyancy to free stream convective buoyancy,

$$F_* = \frac{F_s}{z_i U w_*^2}$$

and for

$$F_s = \frac{g\Delta\rho W_s D_s^2}{4\rho},$$

$$F_* = \frac{Fr_m}{4}\left[\frac{D_s}{z_i}\right]\left[\frac{U}{w_*}\right]^2,$$

F_* was first used to describe plume motion in CBL situations by Briggs (1975). but it has also been affirmed by Kerman (1979), Willis and Deardorff (1983) and Venkatram (1991). When F_* is zero, plume trajectory and dispersion is dominated by convective turbulence, at 0.02 weak buoyancy interactions occur, at 0.05 moderate buoyancy effects are observed, and by 0.10 strong buoyancy effects can be expected.

An attractive characteristic of the buoyancy parameters Fr_m or F_* is that they permit the enhancement of model velocities through distortion of plume density. Indeed, using pure helium as a model plume simulant allows one to increase typical model flow velocities 2.5 times. Model plume Reynolds number also increases by a factor of two, which encourages the emission of a turbulent model plume. The only distortion of scale caused by this modeling is in the kinematic ratios near the plume exit, and mass ratios, which need consideration when determining concentration ratios between model and full scale.

a. Exhaust characteristics of typical power-station plumes

Two typical prototype power stations are considered: the Gladstone Power Station and the Loy Yang or Driffield Power Station, Australia. Consider a sunny day with an inversion height of 1000 m, wind speeds of $U = 4\ ms^{-1}$, and an ambient temperature of $T = 20°C$. Take $Q = 400\ Wm^{-2}$, which corresponds approximately to Pasquill stability class B. Their characteristics are summarized in Table 1. Based on calculated F_* values the Gladstone Station plume will be strongly affected by convective turbulence, whereas the Loy Yang Station plume will be dominated initially by plume buoyancy.

Table 1 Typical Power-station Exhaust Characteristics

Power station:	*Gladstone*	*Loy Yang*
Stack height, h_s (m) =	140	260
Stack diameter, D_s (m) =	6	11
Emission velocity, W_s ($m\ s^{-1}$)	15	28
Emission temperature, T_s (°C)	140	175
Emission density, ρ_s ($kg\ m^{-3}$)	0.851	0.785
Stack density defect, $\Delta\rho$ ($kg\ m^{-3}$)	0.349	0.415
Convective velocity, w_* ($m\ s^{-1}$)	2.23	2.23
Buoyancy flux, F_s ($m^4\ s^{-3}$)	385	2874
Buoyancy parameter, F_*	0.0193	0.145

b. Wind-tunnel simulation conditions for typical power-station plumes

Consider a wind-tunnel simulation where a helium simulant gas is specified. maximum model surface heating rate is 5 KWm^{-2}, and three model scales 750:1, 500:1 and 200:1 are possible. Assume one examines behavior 10 km downwind of the stack for the atmospheric conditions given in section 3-a above. In such circumstances the similitude parameters discussed above reduce to the model data in Table 2.

Table 2 Model conditions to simulate Gladstone and Loy Yang Power Station exhaust plumes.

Model Parameter	*Gladstone Model*			*Loy Yang Model*		
Length Ratio =	750	500	200	750	500	200
x (m) =	13.3	20	50	13.3	20	50
z_i (m) =	1.33	2	5	1.33	2	5
h_s (m) =	0.19	0.28	0.70	0.35	0.52	1.30
D_s (m) =	0.008	0.012	0.030	0.015	0.022	0.055
U (ms^{-1}) =	0.38	0.46	0.73	0.34	0.42	0.66
W_s (ms^{-1}) =	3.21	3.94	6.22	5.18	6.34	10.05
Q (Wm^{-1}) =	254	312	490	184	225	356
w_* (ms^{-1}) =	0.21	0.26	0.41	0.19	0.23	0.37
W_s/U =	8.49	8.49	8.49	15.24	15.24	15.24
w_*/U =	0.56	0.56	0.56	0.56	0.56	0.56
F_s ($m^4 s^{-3}$) =	.00043	0.0012	0.0118	0.0024	0.0065	0.064
Fr_m =	4.01	4.01	4.01	16.3	16.3	16.3
F_* =	0.019	0.019	0.019	0.145	0.145	0.145
MR =	.00036	.00036	.00036	.00039	0.0039	0.0039
Re_s =	214	394	1555	646	1162	4610
x^* =	5.58	5.58	5.58	5.58	5.58	5.58

If one requires model mixed layer velocities greater than 0.5 ms^{-1} and limits the wind tunnel length to 40 m; then wind tunnel models of both the Gladstone and the Loy Yang situations are practical at length-scale-ratios between about 400:1 to 300:1. As required the model and prototype values of convective velocity ratio (w_*/U), stack height ratio (h_s/z_i), buoyancy parameter (F_*), and dimensionless distance ($x^* = xw_*/(z_iU)$) will all be equivalent.

4. Wind-tunnel Operating Range for CBL Simulations

Meteorological wind tunnels are, in effect, analog computers with 'near-infinitesimal' resolution and 'near-infinite' memory (Snyder, 1972). They employ real fluids, not mathematical models of fluids, and produce inherently viscous, turbulent, nonhydrostatic, non-Boussinesq, and compressible flows with no-slip boundary conditions. However, flows in scaled physical models are also only partially similar and cannot at present include all processes present in the atmosphere such as Coriolis acceleration, exchange of energy by radiation, conduction into the soil, and phase changes of water.

Simulation of atmospheric motions by wind-tunnel flows has occurred for almost 100 years since Professor LeCour constructed a wind-mill test facility in Askov, Denmark, in 1895 and Gustaf Eifel designed his exhibition tower in 1889. Background reviews about laboratory simulation were prepared by Cermak (1975), Davenport and Isyumov (1967) and Melbourne (1977). Meroney (1981, 1990) considered the simulation of complex terrain and valley drainage situations. Snyder (1981) suggested similarity criteria for the study of air-pollution meteorology in near neutral situations. Meroney (1987) extended the discussion to the simulation of dense-gas plumes in the surface layer. Meroney et al. (1975) and Avissar et al. (1990) proposed simulation criteria and operating ranges for the simulation of sea and land breezes.

a. General similarity requirements

During physical model simulations of atmospheric flows, scale-model replicas of observed ground-level buildings and terrain are constructed and inserted into a laboratory flow facility. The flow characteristics and stratifications of the air in the wind tunnel are adjusted to be similar as possible to the atmospheric conditions. Complete equivalence of the laboratory model and atmospheric prototype flow fields requires geometric, kinematic, dynamic, and thermal similarity. In addition, boundary conditions upstream, downstream, at the lower surface, and near the top of the physical model must be similar to those at the corresponding boundaries of the modeled atmospheric domain. These multiple similarity requirements, the characteristics of the wind tunnel and its instrumentation, and the nature of the atmospheric phenomenon to be modeled all help to determine the operating range (OR) for a wind-tunnel simulation.

Similarity characterization of stratified atmospheric flows are summarized by Avissar et al. (1990). Specific characterization of CBL phenomena was discussed earlier in Sections 1.1 through 1.4. Equality of these similitude parameters must be supplemented by the requirements that the surface boundary conditions and the approach-flow characteristics also be similar for model and prototype. Boundary-condition similarity requires similar values of

- Surface roughness,
- Topographic relief,
- Surface temperature distribution,
- Upstream distribution of mean and turbulent velocities,
- Upstream distribution of mean and turbulent temperatures, including inversion height, and
- Longitudinal pressure gradient.

If all of the above conditions are met simultaneously, then all scales of motion ranging from the atmospheric microscale to mesoscale could be simulated exactly by the laboratory model. Unfortunately, not all conditions can be satisfied simultaneously by a scaled model since some are incompatible or conflicting; hence, only partial or approximate similarity can be achieved. This suggests that a laboratory model for a particular meteorological situation must be designed to simulate most accurately those scales of motion which are of greatest significance for the application. In the case of a CBL with undistorted horizontal and vertical scales the primary parameters of interest will be w_*/U and inversion height, z_i.

b. Instrumentation Characteristics

Avissar et al. (1990) reviewed wind-tunnel instrumentation characteristics, and they suggested that measurement accuracy was enhanced for model flow speeds of 0.5 m/s and greater. Averaging times and sampling rates may be expected to produce fractional errors of 1, 5 and 10% for averaging times of 400, 16, and 4 seconds, respectively. Conventional sized hot-film instrumentation should produce only a 4% spatial resolution error.

c. Wind-tunnel characteristics

Simulation of the atmospheric CBL is not only a function of the governing flow physics but also depends on the availability of a suitable simulation facility and its instrumentation. In particular the size of the wind-tunnel test section will determine the smallest model length scale ratio (LSR). Most meteorological tunnels range in size from 0.5 x 0.5 m to those with working cross-sections of 3 x 4 m. An exception is the new environmental wind tunnel at Monash with a cross-section of 5 x 10 m. Density stratification can be induced by use of heat exchangers, injection of heated air, gases of different molecular weight, or latent heat absorption or release during phase change (e.g., Ogawa *et. al.*, 1985; Meroney, 1986). By using vortex generators, fences, roughness elements, grids, screens or jets, a wide range of turbulence integral scales can be introduced into the tunnel boundary layer. Choice of model surface roughness or stratification permits control of surface turbulence intensity, dimensionless wall shear, and velocity profile shape.

Two tunnels have been chosen to represent the characteristics of such facilities. The meteorological wind tunnel (MWT) at Colorado State University is a large, closed-circuit facility with a 1.8 m high by 1.8 m wide by 24 m long test section. Wind speeds are continuously variable from 0.1 to 30 m s^{-1} and ambient air temperatures can be varied from 5 to 205°C (e.g. Cermak, 1975, 1982). Ten meters of the upstream floor can be cooled between 1°C and ambient temperature while 12 m of the downstream test-section floor can be heated from 1 to 200°C.

The environmental wind tunnel (EWT) at Monash University is a large, open-circuit facility with a 5-7 m high by 10-12 m wide by 40 m long test section. Wind speeds are continuously variable from 0.1 to 18 ms^{-1} (or to 45 ms^{-1} with cross-section reduced). Ambient air temperatures are drawn into the entrance section, but wall heaters may be inserted to regulate wall temperatures. The wall heaters have a surface heat capacity of 5 kw m^{-2}.

The following criteria have been identified which limit the MWT and EWT operational ranges:

	Colorado State MWT	Monash EWT
@ Maximum model inversion height	< 1 m	< 5 m
@ Maximum inversion strength	< $-10°Cm^{-1}$	< $-10°Cm^{-1}$
@ Minimum model inversion height	0	0
@ Maximum model blockage	< 5 %	< 5 %
@ Minimum plume Reynolds number	> 300	> 300
@ Minimum model wind speed	> 0.5 ms^{-1}	> 0.5 ms^{-1}
@ Maximum model heat flux	< 5 KWm^{-2}	< 5 KWm^{-2}

Coriolis force considerations also limit the maximum acceptable LSR. Snyder (1972) suggests a 5 km maximum cut-off point for horizontal length scales for modeling atmospheric diffusion. Mery *et. al.* (1974) suggests a 15 km limit, Ukeguchi *et al.* (1967) suggest a 40 to 50 km limit, and Cermak *et al.* (1966) proposed a 150 km limit. Given the strong mixing present in CBL situations and time scales of about 3 hours then surface generated stresses should dominate most situations for at least 2 to 5 km.

d. Wind-tunnel performance envelopes for CBL simulations

The most severe restrictions on the wind-tunnel operating range or performance envelope result from geometric similarity constraints. For example Deardorff proposed that laboratory conditions should be sought where $z_i/L_{mo} > 10$ ($z_i/L > 25$) to simulate the mixed layer. Yet the height of most facilities (1-2 m) would limit the dynamic layer to 2 mm, the dynamic convective layer to 2 cm, and the free convection layer to less than 20 cm. Presuming wind-tunnel facilities with model z_i = 1 and 5 m, respectively, then the various characteristic model depths might be:

	Colorado State MWT	Monash EWT
z_i ≈	1 m	5 m,
L_* ≈	0.002 m	0.01 m,
L ≈	0.02 m	0.10 m,
L_{**} ≈	0.04-0.10 m	0.20-0.50 m, and
L_{ASL} ≈	0.04-0.12 m	0.20-0.60 m.

An additional criteria required to avoid secondary circulations imposed by facility size is that the aspect ratio of width to inversion height should be greater than 4. Willis and Deardorff (1974) found that at values of 2, results were no longer consistent with an infinitely large homogenous layer.

Based on the previous discussions, the following seven similarity criteria appear pertinent to the physical simulation of stack plumes dispersing within CBL circulations:

1. $[Ri_B]_m = [Ri_B]_p$ above the inversion;

2. $[w_*/U]_m = [w_*/U]_p$ in the mixed layer;

3. $[h_s/z_i]_m = [h_s/z_i]_p$;

4. $[\rho_s (W_s)^2/(\rho U^2)]_m = [\rho_s (W_s)^2/(\rho U^2)]_p$;

5. $[g\Delta\rho D_s W_s/(\rho U^3)]_m = [g\Delta\rho D_s W_s/(\rho U^3)]_p$;

6. $(Re)_{plume} > Re_{min} = 300$; and

7. Similar upwind velocity, temperature, and turbulence profiles.

In a CBL situation mechanical and thermal turbulence influence one another in the surface layers. In turn this alters the velocity and temperature profiles throughout the CBL. The bulk Richardson number equality (criterion 1) requires that above the CBL inversion

$$LSR = \left[\frac{(\partial T/\partial z)_m}{(\partial\theta/\partial z)_p}\right]^{1/2} \left[\frac{\theta_p}{T_m}\right]^{1/2} \left[\frac{U_p}{U_m}\right],$$

where LSR denotes the prototype-to-model vertical length-scale ratio and subscripts m and p refer to model and prototype conditions, respectively.

The requirement that the convective velocity to advection velocity scale ratio (Criterion 2) is also satisfied implies that

$$LSR = \frac{\beta (z_i)_p Q_m}{(w_*)_p^3} \left[\frac{U_p}{U_m}\right]^3.$$

Similarity of the depth of the CBL (Criterion 3) requires that

$$LSR = \frac{(z_i)_p}{(z_i)_m}.$$

Stipulation that the modeled plume momentum and buoyancy conditions (Criterions 4 and 5) are similar results in the requirement that

$$LSR = \left[\frac{(\rho_s - \rho)_m}{(\rho_s - \rho)_p}\right]\left[\frac{(\rho_s \rho)_p}{(\rho_s \rho)_m}\right]^{1/2} \left[\frac{U_p}{U_m}\right]^2.$$

The plume Reynolds number will be large enough to ensure a fully turbulent plume (Criterion 6) if one stipulates model conditions such that

$$LSR > \frac{(W_s)_p (D_s)_p}{\nu_m \, Re_{min}} \left[\frac{(\rho_s)_p}{(\rho_s)_m}\right]^{1/2} \left[\frac{\rho_m}{\rho_p}\right]^{1/2} \left[\frac{U_m}{U_p}\right].$$

Combining the similarity constraints given by the equations for LSR above with the characteristic sizes and flow capacities of the wind tunnels described in Section 4-c and typical atmospheric CBL and power-plant exhaust conditions noted in Section 3 provides the relationships and data needed to construct the wind-tunnel operating range and to identify reasonable simulation scenarios. Figures 5 through 10 display performance envelopes for the two wind tunnel sizes that are required to produce Pasquill category A, B, and C style CBL stratification, respectively. The shaded areas are excluded per criteria limitations for both CBL and plume rise simulations. Model plumes produced under CBL conditions in the cross-hatched region may not be turbulent. Simulation of the Gladstone or Loy Yang power station plumes must lie along the lines and within the remaining open polygon region.

Although the smaller MWT can marginally reproduce CBL conditions (Poreh and Cermak, 1984: $z_i/L_{mo} \approx 5.6$-10.7), simultaneous simulation of plume behavior as stipulated by MR and F_* will be unlikely if not impossible. Even for the EWT joint simulation of the CBL and stack-plume behavior can only be performed over a limited LSR and U_π range, especially for Pasquill-Gifford A stability situations.

It is concluded that an extensive range of wind-tunnel modeling of the dispersion of large power station and chemical plant plumes, in a highly unstable atmospheric boundary layer could be achieved with a wind-tunnel working section 5 m high by 10 m wide by 40 m long with 1 MW of floor heating. Model length scale ratios would center about 1/200, with the smallest being about 1/400 and the largest 1/100. The limitations at the small scale are Reynolds number and the practicability of controlling very low wind-tunnel speeds. The limitations at the large scale are mainly the enormous heat requirements and size of the facility needed to model adequate downstream distances from the source.

5. Boundary-layer Control Methods for Augmenting CBL Simulation

A special laboratory facility designed to produce CBL simulation at higher wind speeds would be very desirable. E.J Plate, Karlsruhe University, has suggested that it may be possible to reduce the intense surface heat flux required in the laboratory with a combination of wall heating, mass transpiration of hot fluid at the wall, and induced subsidence of the mixing layer by side-wall suction. In the following paragraphs we will examine the conditions required to perform augmented simulation that might successfully simulate the convective boundary layers measured by Kaimal et al. (1976) during field experiments in Minnesota, U.S.A.

a. A one-dimensional model for augmented CBL simulation

To evaluate the viability of boundary control for CBL simulation consider the one-dimensional entrainment models first proposed by Lilly (1979) and later improved by Betts (1974) and Deardorff (1979). They proposed

$$-\langle wt\rangle_i = (dz_i/dt - W_{z_i})\,\Delta\theta$$

where the heat flux, $\langle wt\rangle_i$ is the negative heat flux of entrainment at z_i. Now Deardorff *et al.* (1980) has shown that $-\langle wt\rangle_i = 0.2\langle wt\rangle_s$. Often $\Delta\theta$ is of the order $\Gamma\Delta z_i$ and Δz_i is of the order of $0.2 z_i$. If one assumes that $\langle wt\rangle_s = \langle wt\rangle_{effective} =$

$\langle wt \rangle + W_w(T_m - T_s)$, where W_w is a wall mass transfer rate of air injected at temperature T_s, then

$$\langle wt \rangle + W_w(T_m - T_s) = (dz_i/dt - W_{zi})\Gamma z_i, \text{ or}$$

$$dz_i/dt = [\langle wt \rangle + W_w(T_m - T_s)]/(\Gamma z_i) + W_{zi}, \text{ or}$$

$$(dz_i/dt)/w_* = 0.3/(Ri_*)_{eff} + W_{zi}^+,$$

where $$(Ri_*)_{eff} = 1/[1/Ri_*^{3/2} + 1/Ri_s^{3/2}]^{2/3},$$

$$Ri_* = g\beta\Gamma z_i^2/[g\beta\langle wt \rangle z_i]^{2/3},$$

$$Ri_s = g\beta\Gamma z_i^2/[g\beta W_w(T_m - T_s)\, z_i]^{2/3}, \text{ and}$$

$$W_{zi}^+ = W_{zi}/w_*.$$

In order to maintain the correct mixing layer growth rate in the model one must require

$$[(dz_i/dt)/w_*]_{prototype} = [(dz_i/dt)/w_* - W_{zi}^+]_{model}.$$

When the prototype mixing layer maintains a constant height, then W_{zi}^+ is determined by $(Ri_*)_{eff}$, which can be produced by various combinations of the parameters Ri_* and Ri_s. Figure 11 displays the values of these parameters required to produce various values of $[(dz_i/dt)/w_*]_{prototype}$. Figure 12 specifies combinations of these parameters which produce zero mixing layer growth for different effective Richardson numbers, $(Ri_*)_{eff}$.

Unfortunately, the action of mass addition at the wall which helps to simulate the mixing layer region, also affects the profiles of mean velocity and temperature in the surface layer, $L_{ASL} = 0.1z_i$. As noted by Arya (1982), the surface layer is expected to be a function of both surface and mixing layer scales. The surface layer scales are the friction velocity, u_*, and the friction temperature, θ_*, which are related to the mixing layer scales by the expressions

$$w_*/u_* = \kappa^{-1/3}(-z_i/L_{mo})^{1/3}, \text{ and}$$

$$T_*/\theta_* = \kappa^{1/3}(-z_i/L_{mo})^{-1/3},$$

where κ is the von Karman constant equal to 0.4. Thus, surface layer cnaracteristics are expected to be functions of all of these variables.

Mass addition to unheated boundary layers results in distortion of the velocity and temperature profiles near the wall due to longitudinal momentum deficits. Meroney (1967, 1968) has derived expressions for the velocity and temperature profiles in transpired flow which obey the equations of motion near the wall. One begins with the one-dimensional equations of motion with mass addition, or

$$W(dU/dz) = d\langle -uw \rangle/dz,$$

$$W(dW/dz) = d\langle w^2\rangle/dz + g\Delta\rho/\rho,$$

$$W(dT/dz) = d\langle -wt\rangle/dz, \text{ and}$$

$$dW/dz = 0.0.$$

The continuity equation requires that $W = W_w$ = constant. Prandtl's mixing-length model suggests $\langle -uw\rangle = \kappa^2 z^2 |dU/dz|(dU/dz)$. One can extend this to heat flux by $\langle -wt\rangle = \kappa^2 z^2 |dU/dz|(dT/dz)$. Introducing these closure models into the equations above and integrating once produces,

$$\kappa z(dU/dz)/u_* = (1 + W^+U^+)^{1/2}, \text{ and}$$

$$\kappa z(dT/dz)/\theta_* = (1 + W^+T^+)/(1 + W^+U^+)^{1/2},$$

where $U^+ = U/u_*$, $W^+ = W_w/u_*$ and $T^+ = (T - T_s)/\theta_*$. Meroney (1967, 1968) developed expanded expressions for the transpired boundary layer from these equations including a wake correction and a sublayer term.

In the near wall region proposed by Monin-Obukhov similarity it is conventional to express the dimensionless shear and heat flux in the surface layer as

$$\kappa z(dU/dz)/u_* = \phi_U(z/L_{mo}), \quad \text{and} \quad \kappa z(dT/dz)/\theta_* = \phi_T(z/L_{mo}),$$

where L_{mo} is the Monin-Obukhov similarity length. For unstable flows where L_{mo} is negative a good approximation to the functionals is

$$\phi_T = \phi_U{}^2 = (1 - 15(z/L_{mo}))^{-1/2}.$$

Combining the equations above to account for the joint effects of surface heating and mass transpiration gives,

$$\kappa z(dU/dz)/u_* = (1 + W^+U^+)^{1/2}/(1 - 15(z/L_{mo}))^{1/4}, \text{ and}$$

$$\kappa z(dT/dz)/\theta_* = \frac{(1 + W^+T^+)}{(1 + W^+U^+)^{1/2}(1 - 15(z/L_{mo}))^{1/2}}.$$

These expressions can be integrated to produce the following functions,

$$U_m{}^+ - U^+ = -W^+/(4\kappa^2)F^2 + (1 + W^+U_m{}^+)^{1/2}F/\kappa, \text{ and}$$

$$T^+ = [(1 + W^+T_m{}^+)\exp(-G) - 1]/W^+,$$

where

$$F = \int_{z/Lasl}^{1} [x(1 - 15(L_{ASL}/L_{mo})x)^{1/4}]^{-1}\, dx, \text{ and}$$

$$G = W^+/\kappa \int_{z/Lasl}^{1} [x(1-15(L_{ASL}/L_{mo})x)^{1/2}((1+W^+U_m{}^+)^{1/2} - W^+F/(2\kappa)]^{-1}\, dx.$$

These expressions are integrable for various combinations of W^*, (L_{ASL}/L_{mo}), U_m^*, and T_m^* for the magnitudes of U^* and T^* at various heights, z/L_{asl}.

Figure 13 displays the variation of dimensionless velocity, $U_m^*-U^*$, versus surface layer position for finite wall blowing and surface heating rates. Heating tends to increase turbulence and reduce the velocity profile power-law coefficient. Figure 14 displays the dimensionless temperature variation for finite wall blowing and various surface heating rates. Blowing tends to reduce velocities near the wall and increase the velocity profile power-law coefficient.

b. Augmented wind-tunnel conditions to simulate the CBL

Results from a CBL experiment conducted over a flat site in northwestern Minnesota. USA, are described by Kaimal *et al.* (1976). Eleven sets of data are tabulated for CBL conditions found during the afternoon. For one set of data the values of U_m, T_m, T_s, and dz_i/dt can be estimated from figures provided. For the other cases assumed values for these parameters must be used. Table 3 summarizes the prototype conditions considered. To calculate missing U_m values a constant surface drag of 0.0014 was assumed. Missing T_m and T_s and b values were set to 295°K, 300°K and 0.004 °Km/s, respectively. When missing, dz_i/dt was set to zero. The similarity rules discussed above permits one to calculate model values for heat flux, mass flux and inversion temperature gradient, Γ, once model velocities, temperatures and inversion height are specified.

Use of the mass addition option can reduce the wall heating considerably for only modest wall mass transport. If one assumes the maximum convenient wall surface flux is 200 w m^{-2}, then blowing rates of only 2 to 20 cm s^{-1} are required for U_m = 2 m s^{-1}.

The above-mixing-layer temperature gradients were presumed specified by the stipulation that $(Ri_*)_{eff}$ must be equal to the prototype value. This similitude requirement results in unfortunately large temperature gradients for the higher model wind speeds. Some may be obtainable in the laboratory, others are definitely too large. But the values required for subsidence velocity, W_{z_i}, are generally less than 1 cm s^{-1}. This can be obtained by only mild suction at the wall, or ignored entirely. An alternative would be to use reduced values for model Γ, but definitely suck at the walls of the tunnel to reduce the expected increase in mixing layer growth.

The effect of mass addition on the simulated surface layer profiles may indeed be significant. Bar charts which indicate the order of magnitude of conditions required to simulate the Minnesota experimental cases in a wind tunnel with a one-meter height are shown in Figures 16 through 19. A comparison of profiles for Case 2A1 are found in Figure 18. Near the wall heating will reduce the effects of mass addition to a nearly neutral profile shape, but the dimensionless velocities would still be larger than their prototype counterpart. Temperature profiles of $T^*-T_m^*$ display a similar behavior with heating and blowing. When $W^* = (Ri)_{Lasl} = 0$ then temperature and velocity obey the same equations of motion and boundary conditions; hence, $U_m^*-U^* = T_m^*-T^*$.

6. Conclusions

This paper has examined the characteristics, capabilities, and limitations of meteorological wind tunnels to simulate the atmospheric convective boundary layer. A significant conclusion is that such facilities provide an opportunity to explore CBL sublayer and entrainment layer behavior and an opportunity to examine routine interaction of plumes with CBL turbulence.

Extensive experience with stratified water tanks and wind tunnels definitely suggests that the important turbulence characteristics of the convective boundary layer can be simulated in the laboratory. Nonetheless, laboratory simulation is often not automatic or convenient. Examination of the characteristics of mixing layer entrainment and surface layer behavior determines that:

1. Useful CBL simulations may be obtained in sufficiently large stratified wind-tunnel facilities without augmentation techniques.

2. The use of sufficiently large stratified wind-tunnel facilities will provide a means to study the atmospheric sublayers associated with the CBL.

3. Large to modest wind tunnel mixing layer velocities, $1 < U_m < 2$ m s^{-1}, can be obtained in smaller facilities through the use of floor mass addition and wall suction; however,

4. Large above-mixing-layer model temperature gradients may be required, unless

5. Roof mass addition and side-wall suction is used to reduce the model temperature gradients above the mixing layer.

6. Mass addition and boundary layer control required on the side walls are generally modest requiring cross-flow velocity magnitudes between 0.1 to 25 cm s^{-1}.

7. Mass addition will modify mean velocity and temperature profiles in the surface layer. The additional wall heat flux due to mass addition is not likely to completely compensate for the momentum deficit effects of mass addition.

8. The complication of such boundary-layer-control structures can be avoided if one utilizes very low model mixing layer velocities, $U_m < 0.5$ m s^{-1}. An alternative approach would be to develop hot-film technology, laser specal velocimetry, or laser-anemometry to make such measurements in the lower velocity range.

Acknowledgments

This work was partially supported by the U.S. Office of Naval Research under Contract N00014-88-K-0029.

References

Arya, S.P.S. and Plate, E.J. (1969), "Modeling of the Stably Stratified Atmospheric Boundary Layer," J. Atmo. Sci., Vol. 26, No. 7, pp. 656-665.

Arya, S.P.S. (1982), "Atmospheric boundary layers over homogeneous terrain," Chapter 6 in Engineering Meteorology, ed. E.Plate, Elsevier, New York, pp. 233-268.

Atkinson, J.F. and Harleman, D.R.F. (1983), "A wind-mixed layer model for solar ponds," Solar Energy, Vol. 31, pp. 243ff.

Avissar, R., Moran, M.D., Wu, G., Meroney, R.N., and Pielke, R.A. (1990), "Operating Ranges of Mesoscale Numerical Models and Meteorological Wind Tunnels for the Simulation of Sea and Land Breezes", Boundary-Layer Meteorol., Vol. 50, pp. 227-275.

Betchov, R and Yaglom, A.M. (1971), "Comments on the theory of similarity as applied to turbulence in an unstably stratified fluid," Izv. Akad. Nauk. SSSR, SEr. Fiz. Atmosf. i Okvana, 7, 1270-1279 (829-832 in the English translation of the journal).

Briggs, G.A. (1975), "Plume Rise Predictions" in "lectures on Air Pollution and Environmental Impact Analysis", Workshop Proceedings, Boston, Mass., Sept. 29-Oct 3, 1975, American Meteorological Society, pp. 59-111.

Caughey, S.J. (1984), "Observed Characteristics of the Atmospheric Boundary Layer," Atmospheric Turbulence and Air Pollution Modelling, (ed. F.T.M. Nieuwstadt and H. van Dop), D. Reidel Pub. Co., Boston, pp. 107-158.

Cermak, J.E. (1975), "Applications of Fluid Mechanics to Wind Engineering - A Freeman Scholar Lecture", J. Fluids Eng., Vol. 97, pp. 9-38.

Cermak, J.E., Sandborn, V.A., Plate, E.J., Binder, G.H., Chuang, H., Meroney, R.N. and Ito, S. (1966), "Simulation of Atmospheric Motion by Wind-Tunnel Flows", Report No. CER66-17, May, Department of Civil Engineering, Colorado State University, 101 pp.

Davenport, A. and Isyumov, N. (1967), " The application of the Boundary Layer Wind Tunnel to the prediction of wind loading," Proc. Int. Seminar on Wind Effects on Buildings and Structures, Ottawa, Canada.

Deardorff, J.W. (1970), "Convective velocity and temperature scales for the unstable planetary boundary layer and for Rayleigh convection," J. Atmos. Sci., Vol. 27, pp. 1211-1213.

Deardorff, J.W. (1972), "Numerical investigation of neutral and unstable planetary boundary layers," J. Atmos. Sci., Vol. 29, pp. 91-115.

Deardorff, J.W. (1974), "Three-dimensional numerical study of the height and mean structure of a heated planetary boundary layer," Bound. Layer Meteor., Vol. 7, pp. 81-106.

Deardorff, J. W. (1979), "Prediction of Convective Mixed-layer Entrainment for Realistic Capping Inversion Structure," J. Atmos. Sci., Vol. 36, pp. 424-436.

Deardorff, J.W. and Willis, G.E. (1975), "A Parameterization of Diffusion into the Mixed Layer", J. Appl. Met., Vol. 14, pp. 1305-1458.

Deardorff, J.W., Willis, G.E. and Stockton, B.H. (1980), "Laboratory studies of the entrainment zone of a convectively mixed layer," J. Fluid Mech., Vol. 100, Part 1, pp. 41-64.

Iwasa, Y., Tamai, N. and Wada, A. (1988), Refined Flow Modelling and Turbulence Measurements, Universal Academy Press, Inc., Tokyo, 996 pp.

Kader, B.A. and Yaglom, A.M. (1990), "Mean fields and fluctuation moments in unstably stratified turbulent boundary layers," J. Fluid Mech., Vol. 212, pp. 637-662.

Kaimal, J.C., Wyngaard, J.C., Haugen, D.A., Cote, O.R. and Izumi, Y. (1976), "Turbulence Structure in the Convective Boundary Layer," J. of the Atmos. Sci., Vol. 33, pp. 2152-2169.

Kerman, B.R. (1979), "A Similarity Model for Maximum Ground Level Concentration in a Freely Convective Atmospheric Boundary Layer", Boundary-Layer Meteor., Vol. 16, pp. 395-408.

Lamb, R.G. (1984), "Diffusion in the Convective Boundary Layer," Atmospheric Tubulence and Air Pollution Modelling, (ed. F.T.M. Nieuwstadt and H. van Dop), D. Reidel Pub. Co., Boston, pp. 159-230.

Lilly, D.K. (1968), "Models of cloud-topped mixed layers under a strong inversion," Quart. J. Roy. Meteor. Soc., Vol. 94, pp. 292-309.

Melbourne, W.H. (1977), "Development of Natural Wind Models at Monash University," 6th Aust. Hydraulics and Fluid Mechanics Conference, Adelaide, pp. 190-194.

Melbourne, W.H. (1982), "Atmospheric Dispersion and Wind-wave Test Facility," Monash University, 8 pp.

Melbourne, W.H. (1984), "Progress Report on the Atmopsheric Disperison Modelling Facility to the Electricity Supply Association of Australia," Monash University, 34 pp.

Meroney, R.N. (1967), "Velocity and shear distributions in a transpired turbulent boundary layer", Proceedings of the Tenth Midwestern Mechanics Conference, Colorado State University, Fort Collins, pp. 1125-1143.

Meroney, R.N. (1968), Turbulent sublayer temperature distribution including wall infjection and dissipation", Int. J. Heat Mass Transfer, Vol. 11, pp. 1406-1408.

Meroney, R.N. (1976), "An Algebraic Stress Model for Stratified Turbulent Shear Flows," Computer and Fluids, Vol. 4, pp. 93-107.

Meroney, R.N. (1981), "Physical simulation of dispersion in complex terrain and valley drainage flow situations", Air Pollution Modeling and Its Application, Ed. C. De Wispelaere, Plenum Publishing Co., 21 pp.

Meroney, R.N. (1986), "Wind-tunnel Modeling of Convective Boundary-layer Phenomena," Colorado State University Memorandum CEM86-87-RNM49., 37 pp.

Meroney, R.N. (1987), "Guidelines for Fluid Modeling of Dense Gas Cloud Dispersion", Journal of Hazardous Materials, Vol. 17, pp. 23-46.

Meroney, R.N. (1990), "Fluid Dynamics of Flow over Hills/Mountains--Insights Obtained through Physical Modeling", Chapter 7 of Atmospheric Processes Over Complex Terrain, Ed. W. Blumen, American Meteorlogical Society Monograph No. 45, pp. 145-171.

Meroney, R.N., Cermak, J.E. and Yang, B.T. (1975), " Modeling of Atmospheric Transport and Fumigation at Shoreline Sites", Boundary-Layer Meteorol., Vol. 9, pp. 69-90.

Meroney, R.N. and Melbourne, W.H. (1991), "Operating Ranges of Meteorological Wind Tunnels for the Simulation of Convective Boundary Layer Phenomena," Submitted to Boundary-Layer Meteor., xx pp.

Mery, P., Schon, J.P., and Solal, J. (1974), "Comparison of Thermally Neutral and Unstable Shear Flows in the Wind Tunnel and the Atmospnere", Adv. Geophys., Vol. 18B, pp. 273-287.

Monin, A.S. and Obukhov, A.M. (1954), "Basic laws of turbulent mixing in the atmospheric mixing layer," Trudy Geofiz. Inst. Akad. Nauk SSSR, No. 24 (151), 163-187.

Obukhov, A.M. (1946), "Turbulence in thermally inhomogeneous atmosphere," Trudy Inst. Teor. Geofiz. Akad. Nauk SSSR, No. 1, pp. 95-115 (Transl. in Bound. Layer Meteor., Vol. 3, pp. 7-29, 1971).

Obukhov, A.M. (1960), "Structure of temperature and velocity fields under conditions of free convection," Izv. Akad. Nauk SSSR, Ser Geofiz. No. 9, pp. 1392-1396.

Ogawa, Y., Diosey, P.G., Uehara, K., and Ueda, H. (1985), "Wind Tunnel Observation of Flow and Diffusion uncer Stable Stratification", Atmos. Environ., Vol. 19, pp. 65-74.

Panofsky, H.A., Tennekes, H., Lenschow, D.A. and Wyngaard, J.C. (1977), "The characteristics of turbulent velocity componenets in the surface layer under convective conditions," Boundary-Layer Meteor., Vo. 11, pp. 355-361.

Poreh, M. and Cermak, J.W. (1984), "Wind Tunnel Simulation of Diffusion in a Convective Boundary Layer," Bound. Layer Meteor., Vol. 30, pp. 431-455.

Prandtl, L. (1932), "Meteorologische Anwendug der Stromungslehre," Beitr. Phys. fr Atmos., Vol. 19, pp. 188-202.

Priestly, C.H.B. (1954), "Convection from a large horizontal surface," Austral. J. Phys., Vol. 7, pp. 176-201.

Priestly, C.H.H. (1960), "Temperature fluctuations in the atmospheric boundary layer," J. Fluid Mech., Vol. 7, pp. 375-384.

Rodi, W. (1986), personal communication.

Snyder, W.H. (1972), "Similarity Criteria for the Appication of Fluid Models to the Study of Air Pollution Meteorology", Boundary-Layer Meteorol., Vol. 3, pp. 113-134.

Ukeguchi, N. Sakata, H., Okamato, H., and Ide, Y. (1967), "Study of Stack Gas Diffusion", Tech. Bull. No. 52, Augsut, Mitsubishi Heavy Industries, Ltd., Nagasaki, Japan, 13 pp.

Venkatram, A. (1980), "Dispersion from an Elevated Source in a convective Boudnary Layer", Atmos. Environ., Vol. 14, pp. 1-10.

Willis, G.E. and Deardorff, J.W. (1974), "A laboratory model of the unstable planetary boundary layer," J. Atmos. Sci., Vol. 31, pp. 1297-1307.

Willis, G.E. and Deardorff, J.W. (1983), "On Plume Rise within a Convective Boundary Layer", Atmos. Environ., Vol. 17, pp. 2435-2447.

Wyngaard, J.C. (1988), "Convective Processes in the Lower Atmosphere," Flow and Transport in the Natural Environment: Advances and Applications, (eds. W.L. Steffen and O.T. Denmead), Springer Verlag, Berlin, pp. 240-260.

Table 3: Prototype wind conditions during Minnesota Convective Boundary Layer Experiments of Kaimal *et al.*, 1976

Run Number	*Prototype CBL Parameters, (Kaimal et al., 1976)*							*Dimensionless Parameters*			
	u_* [ms^{-1}]	θ_* [°K]	$-L_{mo}$ [m]	z_i [m]	w_* [ms^{-1}]	T_* [°K]	U_r [ms^{-1}]	Ri_*	U_m/w_*	$-Ri_{\delta m}$	$-z_i/L_{mo}$
2A1	0.45	0.44	41.7	1250	2.00	0.10	12.00	52.0	6.00	3.51	30.0
2A2	0.45	0.46	38.0	1615	2.23	0.09	12.00	69.8	5.38	4.87	42.5
3A1	0.37	0.50	24.0	2310	2.41	0.08	9.87	122.2	4.09	11.05	96.2
3A2	0.32	0.36	24.3	2300	2.06	0.06	8.53	165.8	4.14	10.67	94.7
5A1	0.18	0.38	7.1	1085	1.35	0.05	4.80	85.9	3.56	16.88	152.8
6A1	0.24	0.88	5.7	2095	2.43	0.09	6.40	98.9	2.63	41.52	367.5
6A2	0.23	0.70	6.4	2035	2.21	0.07	6.13	112.8	2.78	35.49	318.0
6B1	0.26	0.28	22.7	2360	1.77	0.04	6.93	236.5	3.92	12.62	104.0
7C1	0.28	0.79	8.8	1020	1.95	0.11	7.47	36.4	3.83	13.51	115.9
7C2	0.30	0.60	13.1	1140	1.89	0.10	8.00	48.4	4.23	10.00	87.0
7D1	0.25	0.40	13.5	1225	1.58	0.06	6.67	80.0	4.22	10.10	90.7

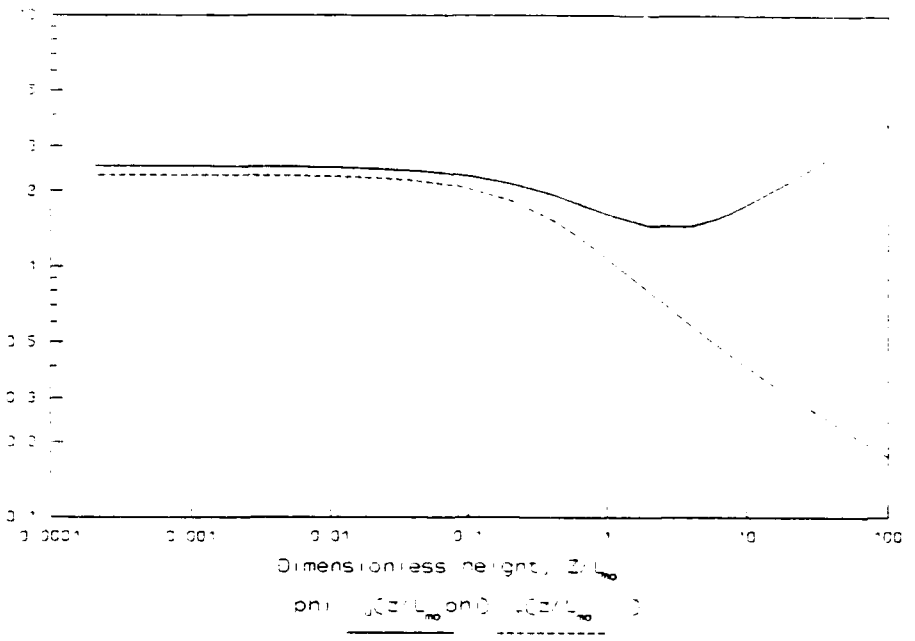

Figure 1 Dimensionless velocity and temperature gradients $\phi_U(\zeta)$ and $\phi_T(\zeta)$ obtained from Kader and Yaglom (1991)--lines are power law expressions.

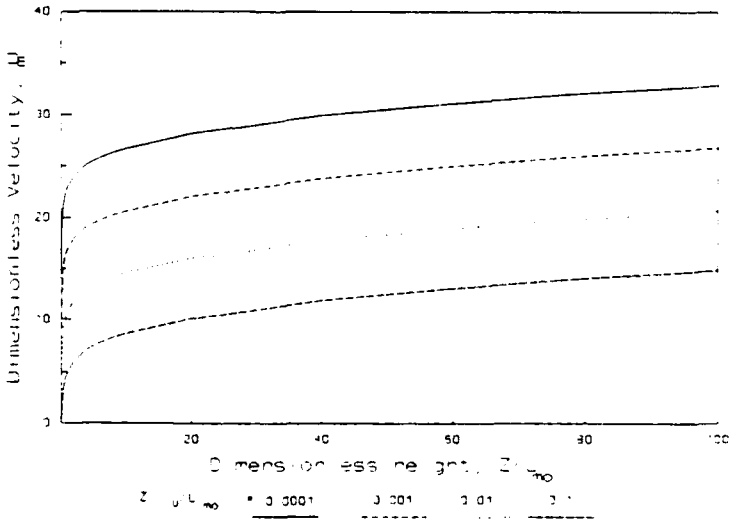

Figure 2 Dimensionless velocity profiles based on Kader and Yaglom (1991) empirical sublayer equations for dimensionless shear.

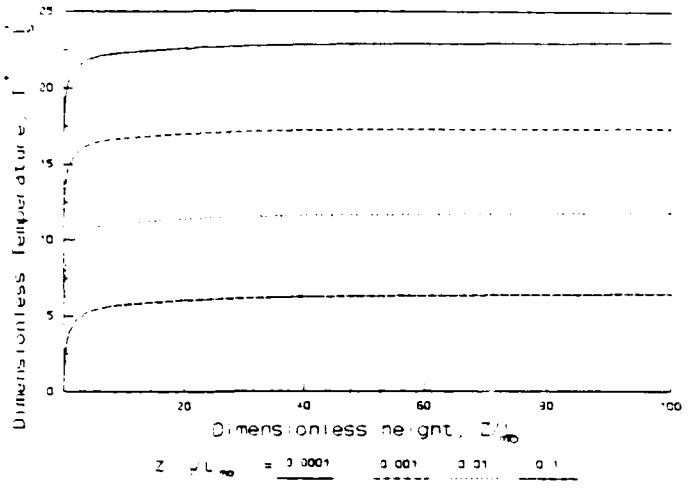

Figure 3 Dimensionless temperature profiles based on Kaglom and Yader (1990) empirical expressions for dimensionless temperature gradient.

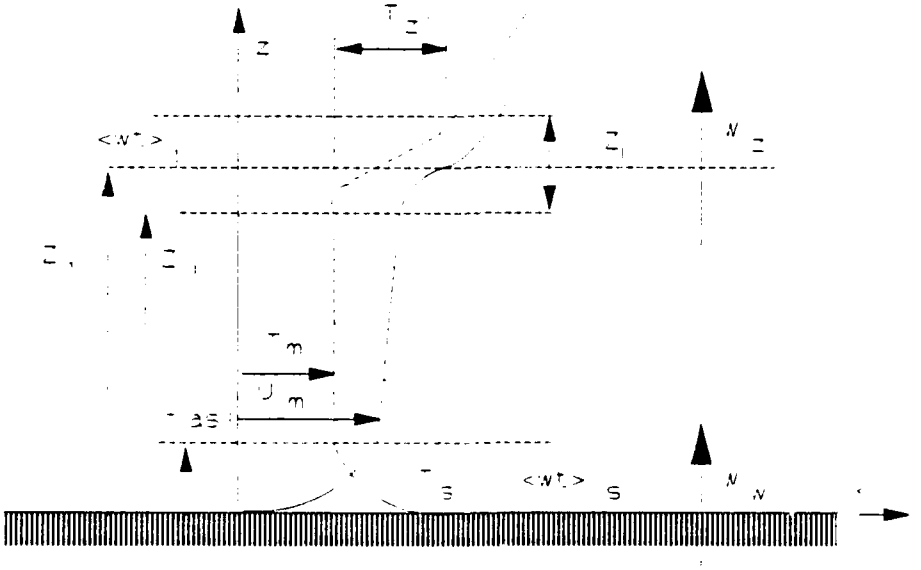

Figure 4 Schematic of the structure of a typical convective boundary layer (CBL)

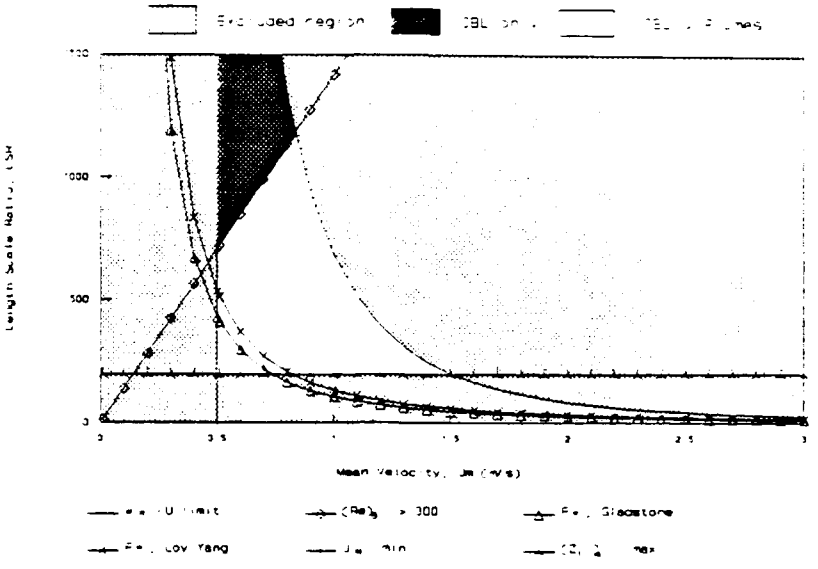

Figure 5 Operating range for CBL simulation of Pasquill Category A conditions in EWT

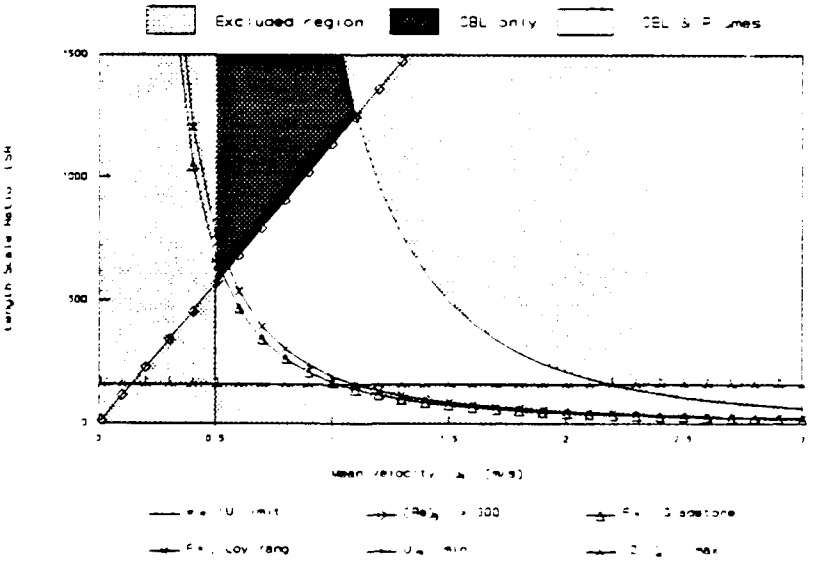

Figure 6 Operating range for CBL simulation of Pasquill Category B conditions in EWT

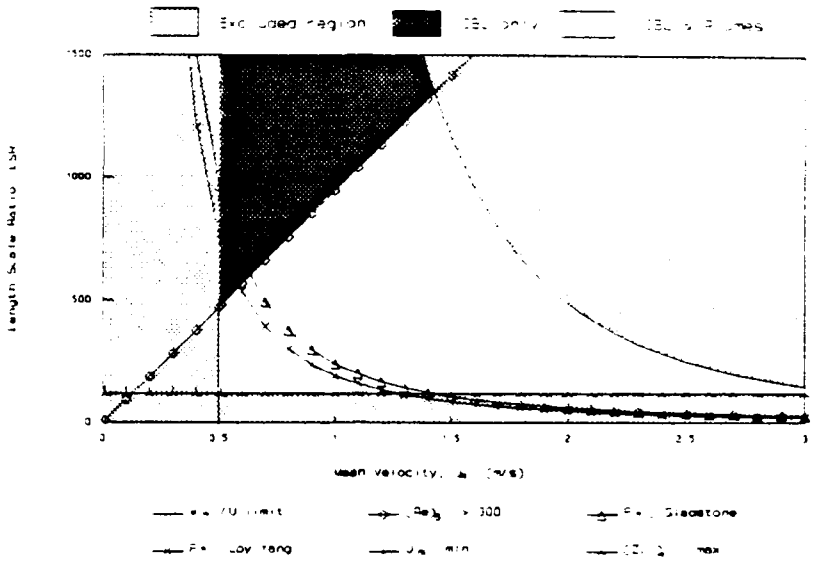

Figure 7 Operating range for CBL simulation of Pasquill Category C conditions in EWT

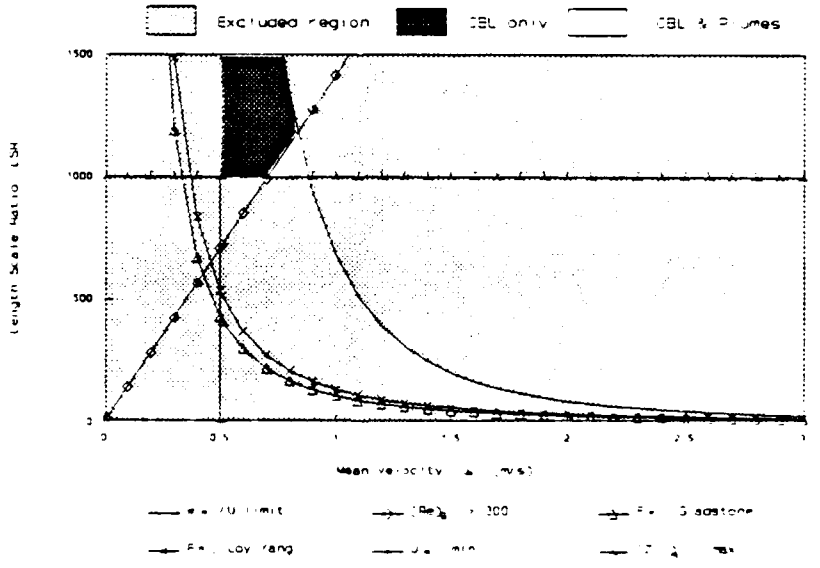

Figure 8 Operating range for CBL simulation of Pasquill Category A conditions in MWT

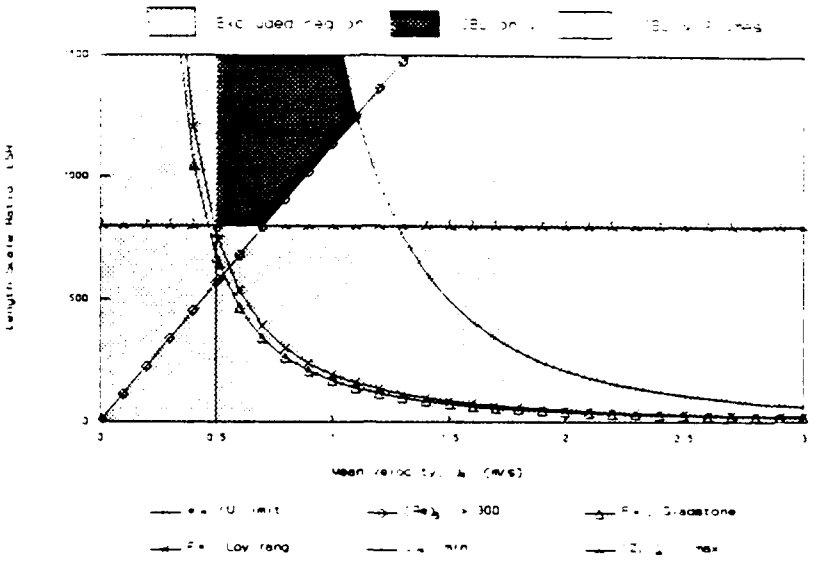

Figure 9 Operating range for CBL simulations of Pasquill Category B conditions in MWT

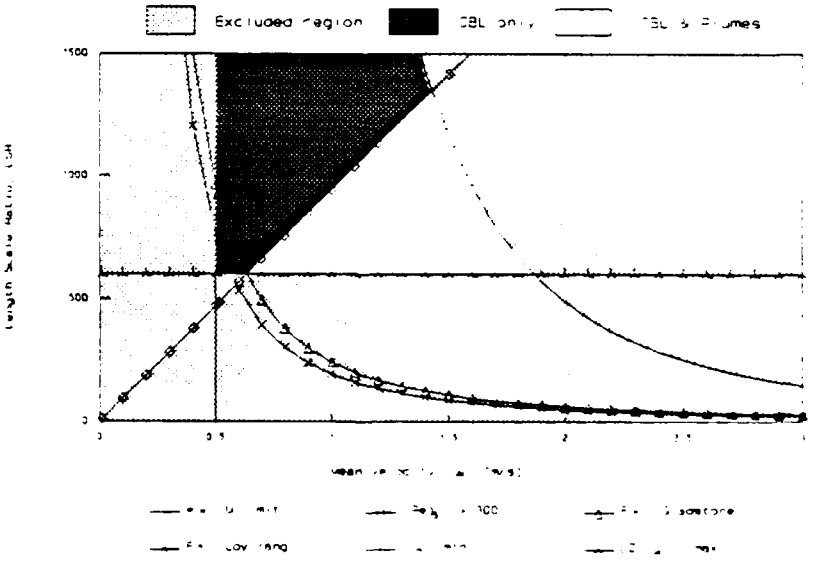

Figure 10 Operating range for CBL simulation of Pasquill Category C conditions in MWT

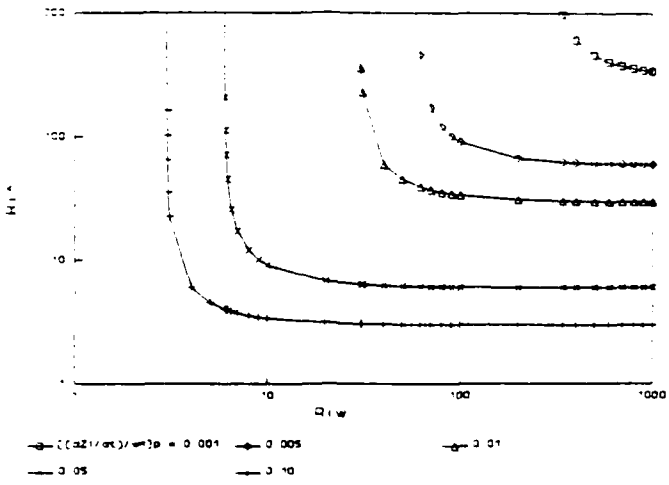

Figure 11 Combinations of surface heat flux and wall mass transfer required to produce specific prototype mixing layer growth rates

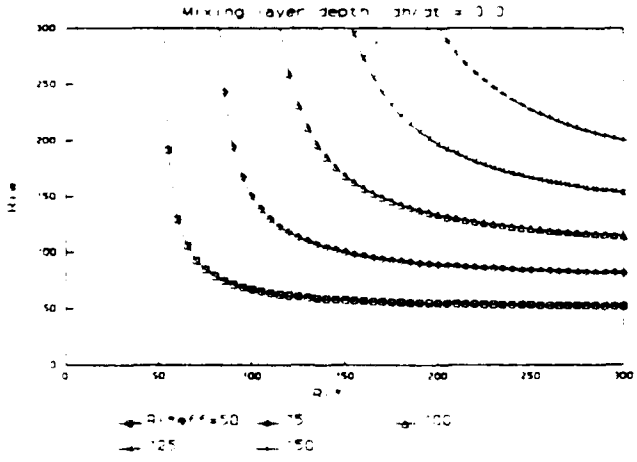

Figure 12 Combinations of surface heat flux and wall mass transfer which produce zero mixing layer growth for different effective Richardson numbers

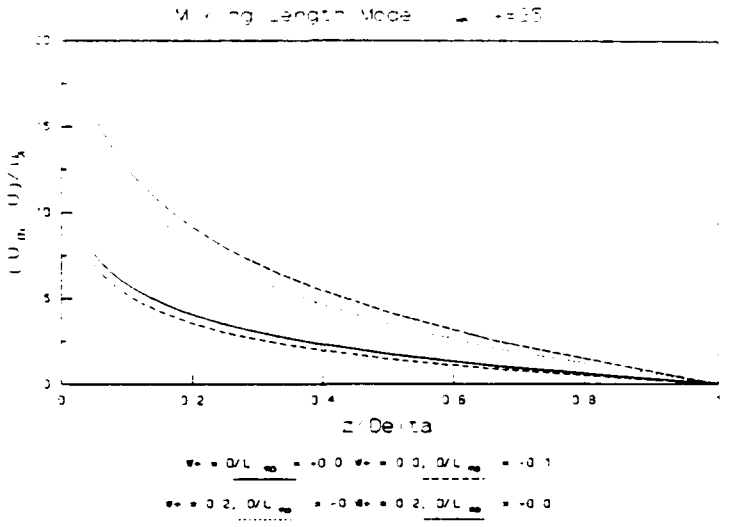

Figure 13 Dimensionless velocity profiles versus surface layer position for finite wall blowing and surface heating rates

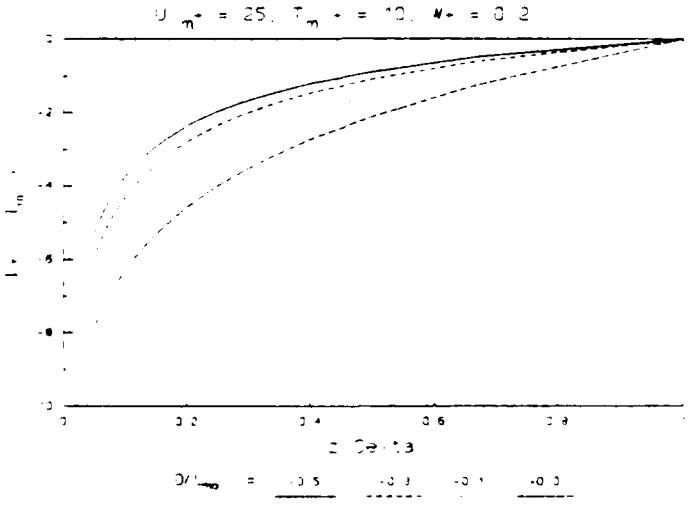

Figure 14 Dimensionless temperature profiles versus surface layer position for finite wall blowing and various surface heating rates

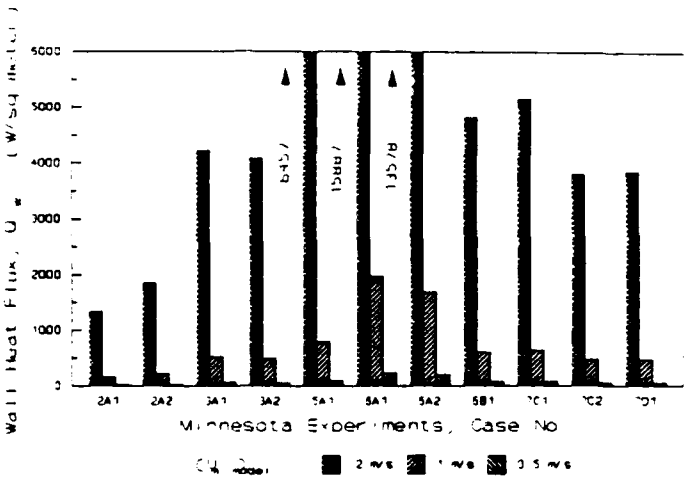

Figure 15 Wall heat flux levels required to simulate Minnesota CBL experiments (Kaimal *et al.*, 1976) for various model mixing layer velocities

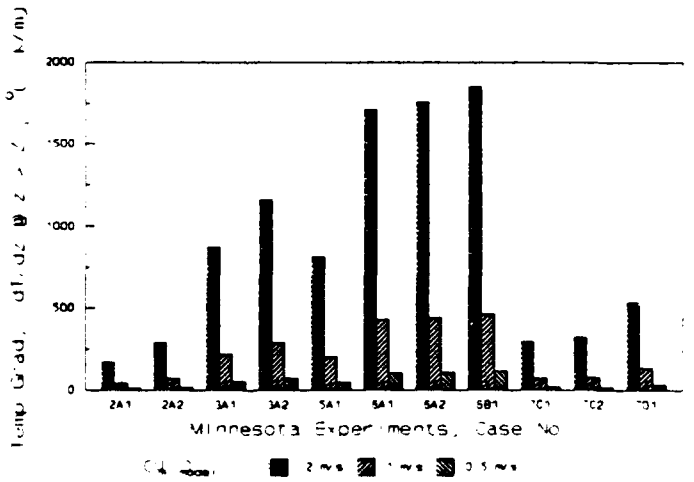

Figure 16 Inversion level temperature gradients required to simulate Minnesota CBL experiments (Kaimal *et al*, 1976) for various model mixing layer velocities

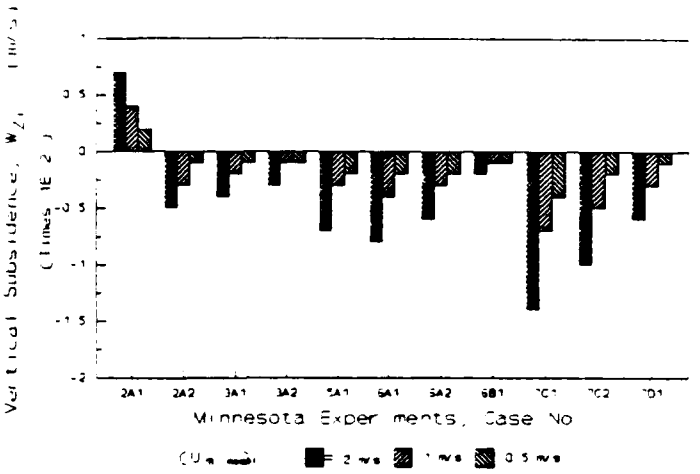

Figure 17 Wind-tunnel subsidence requirements to simulate the Minnesota CBL experiments (Kaimal et al., 1976) for various model mixing layer velocities

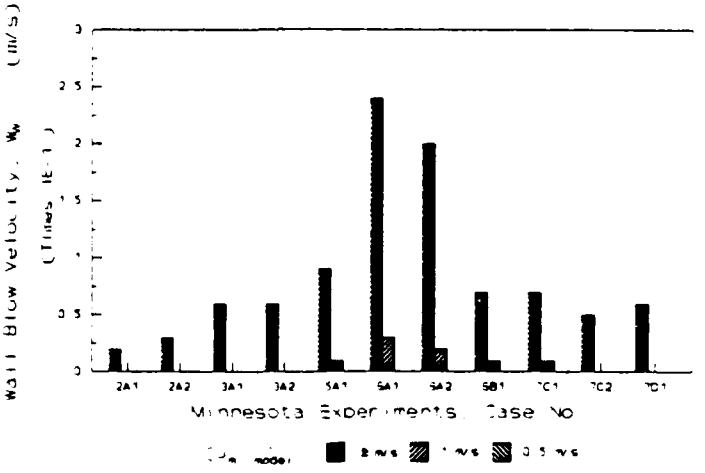

Figure 18 Wind-tunnel wall mass transfer rates required to simulate the Minnesota CBL experiments (Kaimal *et al.*, 1976) for various model mixing layer velocities

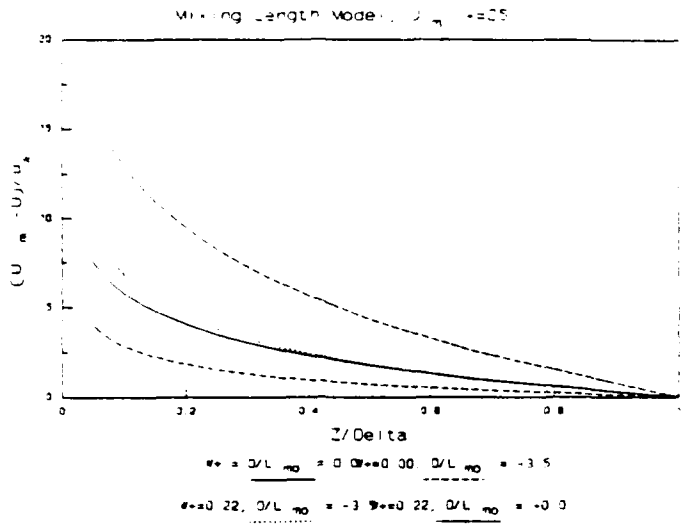

Figure 19 Calculated velocity profiles anticipated in the surface layer when simulating Minnesota Case 2A1 (Kaimal *et al.*, 1976) by augmented wall transport methods